Check for updates

ARTICLE   OPEN

Spin liquid and ferroelectricity close to a quantum critical point in PbCuTe₂O₆

Christian Thurn [1✉], Paul Eibisch[1], Arif Ata[1], Maximilian Winkler [2], Peter Lunkenheimer [2], István Kézsmárki[2], Ulrich Tutsch[1], Yohei Saito[1], Steffi Hartmann[1], Jan Zimmermann[1], Abanoub R. N. Hanna [3,4], A. T. M. Nazmul Islam[4], Shravani Chillal [4], Bella Lake [3,4], Bernd Wolf[1] and Michael Lang[1]

Geometrical frustration among interacting spins combined with strong quantum fluctuations destabilize long-range magnetic order in favor of more exotic states such as spin liquids. By following this guiding principle, a number of spin liquid candidate systems were identified in quasi-two-dimensional (quasi-2D) systems. For 3D, however, the situation is less favorable as quantum fluctuations are reduced and competing states become more relevant. Here we report a comprehensive study of thermodynamic, magnetic and dielectric properties on single crystalline and pressed-powder samples of PbCuTe₂O₆, a candidate material for a 3D frustrated quantum spin liquid featuring a hyperkagome lattice. Whereas the low-temperature properties of the powder samples are consistent with the recently proposed quantum spin liquid state, an even more exotic behavior is revealed for the single crystals. These crystals show ferroelectric order at $T_{FE} \approx 1$ K, accompanied by strong lattice distortions, and a modified magnetic response—still consistent with a quantum spin liquid—but with clear indications for quantum critical behavior.

INTRODUCTION

Competing interactions combined with strong quantum fluctuations are considered a major guiding principle for the realization of a quantum spin liquid. This long sought state of matter is characterized by exciting properties such as macroscopic entanglement and fractionalized excitations, see refs. [1–5] for recent reviews. As quantum fluctuations are enhanced for low spin values and low lattice coordination, most efforts have been devoted to low-dimensional (low-D) quantum spin ($S = 1/2$) antiferromagnets, with prominent examples including the 2D kagome system Herbertsmithite[6,7] and some layered triangular-lattice charge-transfer salts[8–10]. For 3D lattices, the search has focused on materials where the spins reside on a pyrochlore[11,12] or hyperkagome lattice[13], a 3D network of corner-sharing triangles. As in 3D competing ground states are expected to become more relevant, perturbations from purely Heisenberg spin scenarios due to, e.g., Dzyaloshinskii–Moriya interaction[14,15] or spin-orbit coupling[16] gain in importance and may eventually govern the materials' ground state[1]. This raises the general question about the stability of a quantum spin liquid phase in 3D. In fact, for Na₄Ir₃O₈, a 3D effective $S = 1/2$ spin liquid candidate system with a hyperkagome lattice[13], evidence was reported for a nearby quantum critical point[17]—a $T = 0$ instability to some nearby (possibly magnetically) ordered state. More recently, PbCuTe₂O₆ has attracted considerable interest as another 3D quantum spin liquid candidate system featuring a highly-connected hyperkagome lattice[18–20], where $S = 1/2$ Cu²⁺ spins are coupled by isotropic antiferromagnetic interactions. According to magnetic studies, mainly on pressed-powder samples[18–20], this system lacks long-range magnetic order down to 0.02 K[19] and shows diffuse continua in the magnetic spectrum[20] consistent with fractional spinon excitations. Puzzling issues relate to the appearance of small anomalies in the powder samples around 1 K of unknown

origin[18–20] and signs of a phase transition around this temperature in first-generation single crystals[20].

In the present work, we present a comprehensive study of thermodynamic, magnetic and dielectric properties of PbCuTe₂O₆, with special focus lying on its low-temperature state. To this end, we have investigated several single crystals and compare the results with data on pressed-powder samples. The salient results of our study are (i) the observation of a phase transition in single crystalline material around 1 K into a ferroelectrically-ordered state, which is accompanied by strong lattice distortions. (ii) This phase transition and the state at $T \leq 1$ K are characterized by a finite magnetic susceptibility without any indication for long-range magnetic order consistent with a gapless quantum spin liquid state. (iii) The bulk ferroelectric transition and its accompanying lattice distortions are absent in the powder samples. (iv) For these powder samples, the ratio a/C_e, with a the thermal expansion coefficient and C_e the electronic specific heat, probing the thermal Grüneisen parameter Γ_p, is practically independent of temperature for $T \leq 1.6$ K. In contrast, a corresponding uniaxial Grüneisen parameter for the single crystals shows a strong increase for $T \rightarrow 0$, potentially indicating quantum critical behavior. In fact, clear evidence for a nearby field-sensitive quantum critical point is observed in the electronic magnetic Grüneisen parameter $\Gamma_{B,e}$, yielding a divergence for $T \rightarrow 0$.

RESULTS

Material, crystal structure, and magnetic interactions

PbCuTe₂O₆ crystallizes in a non-centrosymmetric cubic structure with space group P4₁32 (No. 213), see Supplementary Fig. 1 and Note 1. According to density functional theory calculations[20] based on room-temperature structural data, the magnetic lattice can be described by isolated equilateral $S = 1/2$ triangles with

¹Physikalisches Institut, J.W. Goethe-Universität Frankfurt(M), Max-von-Laue-Str.1, 60438 Frankfurt, Germany. ²Experimentalphysik V, Zentrum für Elektronische Korrelationen und Magnetismus, Universität Augsburg, Universitätsstr. 1, 86159 Augsburg, Germany. ³Institut für Festkörperforschung, Technische Universität Berlin, Hardenbergstr. 36, 10623 Berlin, Germany. ⁴Helmholtz-Zentrum Berlin für Materialien und Energie, Hahn-Meitner Platz 1, 14109 Berlin, Germany. ✉email: Thurn@Physik.uni-frankfurt.de

nearest-neighbor interaction $J_1 = 1.13$ meV, which are coupled via the second-nearest neighbor interaction $J_2 = 1.07$ meV into a hyperkagome lattice. The weaker third- and fourth-nearest neighbor interactions $J_3 = 0.59$ meV and $J_4 = 0.12$ meV couple the spins into chains. Another special feature of $PbCuTe_2O_6$, which has been largely ignored until now, relates to its dielectric degrees of freedom[21]. The material contains polar building blocks originating from the free electron pairs (lone pairs) of the Te^{4+} ions in the oxotellurate tetrahedrons and the asymmetrically coordinated Pb^{2+} ions. These characteristics together with the non-centrosymmetric structure imply the possibility of ferroelectric order interacting with the strongly frustrated quantum spin system. In fact, a magneto-dielectric effect was observed in $SrCuTe_2O_6$[22] which is isostructural to $PbCuTe_2O_6$ but features a magnetic network with predominantly 1D character.

Measurements were performed on single crystals (sc) from four different batches grown by utilizing two different techniques (see "Methods" and ref. [23]), and pressed-powder (pd) samples (see "Methods") from the same batch prepared as described in ref. [20]. In what follows, the samples will be specified by giving their batch number followed by an alphabetic character to distinguish different samples from the same batch.

Thermodynamic properties

Figure 1 shows the results of the electronic specific heat, C_e, measured on single crystal sc #5(b). The data reveal a pronounced λ-shape phase transition anomaly around 1 K, signaling a second-order phase transition, on top of a broad maximum. The figure also includes data for a pressed-powder sample pd #I(b) showing a distinctly different behavior. Here we find the broad maximum in $C_e(T)$ centered around 1.4 K, followed by a smooth reduction upon further cooling similar to previous reports on powder
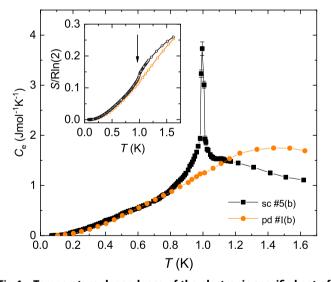
material[18–20]. As also revealed in these studies, we observe signatures for a tiny feature around 1 K and a $C_e(T) \propto T^n$ dependence with $n \approx 2$ at low temperatures $T \leq 0.4$ K.

More insight into the nature of the phase transition in the single crystalline material can be obtained by studying the elastic properties via thermal expansion measurements, cf. Fig. 2. In the inset of Fig. 2, we show data of the relative length changes, $\Delta L_i(T)/L_i$ for sc #1(a) measured along two different directions. Based on structure determination at room temperature, we refer to these directions as $i = [100]$ and $[1–10]$. For the data at higher temperatures down to about 1.7 K, we find a smooth isotropic reduction of $\Delta L_i(T)/L_i$ with decreasing temperature, consistent with a cubic structure. However, on further cooling the thermal contraction becomes increasingly stronger and develops a pronounced anisotropy, indicating deviations from cubic symmetry at low temperatures. At around 1 K we find a sharp break in the slope in $\Delta L_i(T)/L_i$ along both directions, consistent with a second-order phase transition. We stress that the evolution of a nonisotropic lattice strain from a cubic high-temperature state implies the formation of structural domains. As a result, the $\Delta L_i(T)/L_i$ data for $T \leq 1.7$ K in Fig. 2 could potentially be affected by the material's domain structure. In general, the formation of domains can be influenced by the application of uniaxial pressure to the crystal in its high-temperature phase. This is actually the case in our thermal expansion measurements along the measuring direction, where uniaxial pressure of typically 0.01–5 MPa is applied, depending on the sample geometry and the chosen starting capacitance[24], see also "Methods" and Supplementary Note 3. In the main panel of Fig. 2 we show the coefficient of thermal expansion $\alpha_i(T) = 1/L_i \cdot d(\Delta L_i(T))/dT$ for single crystal sc #5(c) along the [110] direction. Since in this experiment a rather high uniaxial pressure of about (6.5 ± 1.3) MPa was realized, we believe that these $\alpha_{[110]}$ data represent a preferential domain orientation
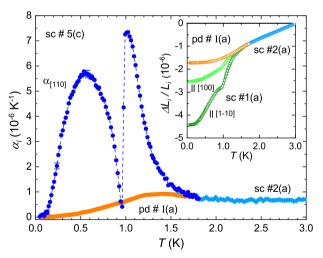

Fig. 1 Temperature dependence of the electronic specific heat of $PbCuTe_2O_6$. Electronic specific heat of single crystal sc #5(b) (black squares) and a pressed-powder sample pd #I(b) (orange spheres). Thin solid lines serve as guides to the eyes. Very similar results to those on sc #5(b) were obtained on a second single crystal #1(b) studied in this experiment, which was grown using a different technique, see "Methods" and Supplementary Fig. 2. For the nuclear contributions subtracted, see "Methods" and Supplementary Fig. 2 and Note 2. Error bars represent the standard deviation due to statistical treatment of raw data. The inset shows the entropy in units of $R\ln2$ for both samples using the same color code. The arrow marks the position of the phase transition anomaly in $C_e(T)$. The entropy release associated with the phase transition over a narrow temperature window of about 0.2 K amounts to a few percent of $R\ln2$.

Fig. 2 Temperature dependence of the coefficient of thermal expansion of $PbCuTe_2O_6$. Thermal expansion coefficient α for single crystal sc #5(c) (dark blue spheres) and sc #2 (light blue diamonds for $T \geq 1.5$ K), both measured along the [110] direction, together with data for the pressed-powder sample pd #I(a) (orange spheres). Broken line serves as a guide to the eyes. Representative error bars resulting from the statistical treatment of raw data and systematical uncertainties related to the determination of the sample length. Error bars of measurement for pd sample are within symbol size. The inset shows relative length changes $\Delta L_i(T)/L_i$ for sc #1(a), measured along [100] (light green triangles) and [1–10] (dark green squares), sc #2 (light blue diamonds) for $T \geq 1.5$ K, and for the powder sample pd #I(a) (orange spheres). The pronounced anomaly in $\alpha_{[110]}$ for $T \leq 1.5$ K is consistent with a strong decrease observed in the longitudinal elastic constant $c_{L[110]}$ upon cooling, see Fig. 8 and Note 5 in Supplementary.

coming close to a mono-domain structure, see Fig. 6 in the Supplementary. Therefore, we confine the discussion of the temperature dependence to these $a_{[110]}$ data. Upon cooling, $a_{[110]}$ shows an extraordinarily strong increase followed by a sharp negative phase transition anomaly slightly below 1 K, and a second maximum around 0.5 K. However, a comparison with the results of $C_e(T)$ for the single crystal sc #5(b) in Fig. 1, showing a maximum around 1 K, suggests another interpretation: there is only a single huge maximum in $a_{[110]}$ centred slightly below 1 K to which a negative λ-shape phase transition anomaly around 1 K is superimposed. The somewhat larger width of the phase transition anomaly in $a_{[110]}(T)$ as compared to $C_e(T)$, may indicate some remaining domain misalignment in the thermal expansion experiment, cf. the narrowing of the phase transition anomaly in $a_{[110]}$ on increasing the uniaxial pressure in Fig. 6 of the Supplementary. Figure 2 also shows thermal expansion data taken on the pressed-powder sample pd #I(a). Whereas the $\Delta L(T)/L$ data for the powder match with the data for the single crystal for $T > 1.6$ K, (see inset of Fig. 2) they deviate at lower temperatures: instead of the strong contraction observed for the single crystal on approaching the phase transition, the powder sample shows a rather smooth behavior with $\Delta L(T)/L$ gradually levelling off upon cooling. The corresponding $a(T)$ data for the powder sample shown in the main panel of Fig. 2 reveal a broad maximum around 1.4 K followed by a smooth variation $a(T) \propto T^n$ with $n \approx 2$ for $T \leq 0.4$ K.

Dielectric constant and polarization

Given the material's non-centrosymmetric structure and its polar building blocks, comprising two subsystems of stereochemically active lone pairs associated with the Te^{4+} and Pb^{2+} ions, the observation of a lattice distortion suggests an involvement of the electric degrees of freedom. To probe the dielectric response, measurements of the dielectric constant were performed on single crystals #1(a), #4 and #5(b) for temperatures $T \leq 1.3$ K. In Fig. 3 we show exemplarily the results of the normalized dielectric constant ε' for sc #5(b). The data reveal an enhanced background dielectric constant of $\varepsilon'_b \approx 18$ in the temperature range investigated and a well-pronounced peak centred at 0.97 K, signaling a ferroelectric transition at $T_{FE} = 0.97$ K. This assignment is further corroborated by a Curie-Weiss-like behavior on approaching the maximum in ε' from both sides, see inset (a) of Fig. 3. In the inset (b) of Fig. 3 we show the frequency dependence of the dielectric anomaly around 1 K. The measurements, covering approximately two decades in frequency, reveal a distinct suppression of the peak with increasing frequency whereas the position of the peak remains essentially unchanged. This behavior is typical for an order-disorder-type ferroelectric transition[25,26] where electric dipoles that are disordered at high temperature order with a net overall polarization below T_{FE}. In contrast, for the pressed-powder sample pd #I(b) we find only a tiny anomaly in ε' around 1 K, see Fig. 3. This observation together with the smooth variation of $\Delta L(T)/L$ for $T \leq 1.6$ K for the powder sample, reflecting the absence of an anomalous lattice distortion as revealed for the single crystals, indicate that there is no bulk ferroelectric transition in the pressed-powder sample.

To further corroborate the ferroelectric nature of the transition detected at about 1 K, we have investigated the polarization P of single-crystalline PbCuTe$_2$O$_6$ (sc #1(a), $E\|[110]$). Figure 4 shows $P(T)$ as measured upon heating after poling the sample with different electrical fields during a preceding cooling run as noted in the figure. Without poling field, no significant polarization was detected, consistent with a multi-domain polar state with even distribution of polarization directions. Prepoling with positive fields between 0.1 and 2.3 kV/cm reveals a successively increasing low-temperature polarization, vanishing above $T_{FE} \approx 1$ K. The observed gradual increase of $P(T)$ below T_{FE} is in accordance with
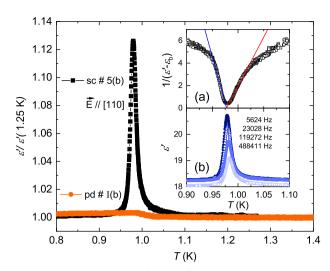

Fig. 3 Temperature dependence of the dielectric constant of PbCuTe$_2$O$_6$. Dielectric constant of single crystal sc #5(b) (black squares), with electric field **E** applied along the [110] direction, and a pressed-powder sample pd #I(b) (orange spheres). Similar measurements on the single crystals #1(a) and #4 reveal essentially the same results albeit with a somewhat reduced peak height, see Supplementary Fig. 9 and Note 6. The inset gives details of the data for sc #5(b) in a narrow temperature range around 1 K. Inset **a**, showing $1/(\varepsilon' - \varepsilon'_b)$ vs. T, reflects a Curie–Weiss-like behavior on approaching the maximum in ε' from both sides. The slopes of the linear regimes differ by a factor of about -1.9. This factor is very close to -2, expected for a mean-field second-order ferroelectric transition[43], but strongly departs from -8 seen at first-order ferroelectric transitions[25,44]. The lower inset **b** shows ε' vs. T for varying frequencies as indicated in the figure. The small shift of the background dielectric constant ε'_b, visible for the data at highest frequency, indicates some contribution from extrinsic factors.
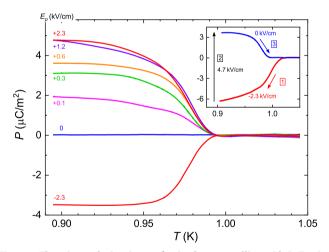

Fig. 4 Electric polarization of single crystalline PbCuTe$_2$O$_6$. Temperature dependence of the electric polarization of single crystalline PbCuTe$_2$O$_6$ (sc #1(a)) as deduced from the pyrocurrent monitored upon heating. The measurements were performed for different poling fields (-2.3 to $+2.3$ kV/cm), applied to the sample along the [110] direction during the preceding cooling run. For original pyrocurrent data taken at different heating rates and poling fields, see Supplementary Fig. 10a and Fig. 10b. The results in the inset demonstrate the switching of the polarization achieved by first cooling the sample within negative field (1), applying a positive field for 1 min at 0.9 K (2), and finally reheating it without field (3).

a second-order nature of the polar phase transition consistent with results of the specific heat and thermal expansion (Figs. 1 and 2). Between 1.2 and 2.3 kV/cm, P exhibits only weak variation with field, pointing to a mono-domain state with saturation polarization of the

order of 5 µC/m². As revealed by the lowest curve in Fig. 4, a negative field of −2.3 kV/cm results in a negative polarization, reflecting a polarization into the opposite direction, as expected for ferroelectrics. The absolute value of P, reached for −2.3 kV/cm is somewhat reduced compared to +2.3 kV/cm which may arise from strains within the crystal, slightly favoring one polarization direction.

Another defining property of ferroelectrics is the switchability of the polarization by an electrical field at temperatures below the transition. For the present material, this is demonstrated in the inset of Fig. 4. In this experiment, the sample was first polarized by cooling it to 0.9 K under negative electrical field of −2.3 kV/cm and then applying a positive field of 4.7 kV/cm. The subsequent heating run without field revealed positive polarization, unequivocally proving the in-situ switching of the polarization within the ferroelectric state.

It should be noted that the detected saturation polarization P_s of $PbCuTe_2O_6$ of about 5 µC/m² ($=0.5$ nC/cm²) is rather small compared, e.g., to the well-established lone-pair ferroelectric $BiFeO_3$[27] or to classical displacive ferroelectrics like $BaTiO_3$[28], revealing P_s values of several tens of µC/cm². This is consistent with the rather small amplitude of the anomaly observed in the dielectric constant at the transition (Fig. 3). Small values of $\varepsilon'(T)$ and P_s are, e.g., also found in some improper ferroelectrics like $TbMnO_3$[29]. However, it is conceivable that P_s is higher for field directions other than the presently used **E**||[110] geometry. To clarify this question, systematic investigations with different contact geometries and/or crystal cuts have to be performed, which is out of the scope of the present work.

$PbCuTe_2O_6$ has a cubic chiral but non-polar crystal structure at high temperatures (space group $P4_132$). Consequently, the onset of ferroelectricity is necessarily accompanied by the lowering of the crystal symmetry. The highest-symmetry polar subgroups of the parent cubic group are the tetragonal $P4_1$ group and the rhombohedral $R3$ group. Though both space groups are compatible with the presence of ferroelectricity, we expect the rhombohedral one being realized in this compound for the following reason: The cubic to rhombohedral distortion maintains the three-fold symmetry of the kagome lattice, while in case of the cubic to tetragonal distortion the kagome lattice would not be regular anymore. Thus, the former would preserve a high degree of frustration of the spin-spin interactions, while the latter would reduce it and by this likely promotes the onset of magnetic ordering, not observed experimentally. Again, future polarization measurements along different crystallographic directions should help clarifying this issue.

DISCUSSION

The different dielectric and lattice properties observed here for the pressed-powder material as opposed to the single crystals, can be rationalized by considering that the powder samples studied here and in the literature[18–20] were all prepared by a solid-state reaction method where the material is subject to multiple grinding processes interrupted by special heat treatments. Correspondingly, these samples constitute a more or less homogeneous collection of grains with some distribution of grain sizes, which may vary from sample to sample and the heat treatment applied. Our finding of a ferroelectric transition in the single crystalline material and the suppression of this transition in the pressed-powder samples is consistent with results on grain-size effects in ferroelectric ceramics (see, e.g., refs. [30–32] and Supplementary Note 7), yielding a critical grain size below which the transition disappears. Triggered by the results of the present work, the influence of the grain size on the 1 K phase transition in $PbCuTe_2O_6$ was systematically investigated in ref. [23]. In their studies, the low-temperature specific heat on single- and polycrystalline samples was measured both after crushing the samples (thereby reducing the size of the crystallites) and after annealing them (thereby increasing the size of the

crystallites and reducing dislocations and grain boundaries). According to ref. [23], the phase transition anomaly around 1 K is drastically reduced for crystallites of diameter 30 µm, and completely vanishes for diameters below 10 µm.

The drastic reduction of the anomaly in ε' around 1 K for the powder sample, together with the smooth behavior in the specific heat and thermal expansion (Figs. 1 and 2) are fully consistent with the absence of a bulk ferroelectric transition and the accompanying lattice distortion in the powder sample. At the same time, as demonstrated by various advanced magnetic measurements[19,20], these powder samples lack long-range magnetic order down to temperatures as low as 0.02 K, indicating that in the non-distorted cubic low-temperature state of $PbCuTe_2O_6$, the frustration of the magnetic network is strong enough to suppress long-range ordering consistent with the formation of a quantum spin liquid state. This raises the question to what extent the magnetic lattice and thus the degree of frustration is altered by the lattice distortions revealed in single crystalline material. In this context it is interesting to note that the broad maximum in the low-temperature specific heat, a feature which is considered a hallmark of strongly frustrated spin systems[13,17,18,33,34], shows a considerable shift from $T_{max} \approx 1.4$ K for the powder sample to below 1 K for the single crystalline material. It is tempting to assign this shift to alterations of the exchange coupling constants in the frustrated spin system in the single crystals due to ferroelectric ordering. This is consistent with results for the magnetization $M(T)$ derived from ac-susceptibility measurements on single crystal #5 (b) (see inset of Fig. 4 and Supplementary Fig. 7 as well as Note 4), still lacking any indication for long-range order for $T \geq 0.1$ K, which reveal a mild reduction of $M(T)$ with decreasing temperatures below about 0.8 K. In contrast, for powder material a slight increase was observed for $M(T)$ on cooling below 1 K[19]. We attribute the change in the magnetic couplings to the lattice distortions—a displacement of the Pb^{2+} ion out of its high-symmetry position—accompanying the ferroelectric transition, see Supplementary Fig. 1d. This displacement allows for a (sp) hybridization with oxygen p orbitals and the formation of a lone pair with asymmetric electron distribution. As these oxygen p orbitals are also involved in the dominant magnetic exchange paths (Supplementary Fig. 1c), we expect changes in the coupling constants J_1 and J_2 of the distorted structure.

Another even more pronounced difference in the materials' low-temperature magnetic/electronic state becomes apparent by studying the ratio $\alpha_{[110]}/C_e$ for sc #5, a quantity which is proportional to the uniaxial thermal Grüneisen parameter $\Gamma_{p[110]}$ (see ref. [35]) and compare this to α/C_e for the pressed-powder sample pd #I, cf. inset of Fig. 5. Note, since for $T \lesssim 1$ K the lattice contribution to α is very small, its influence can be neglected in discussing the critical behavior of the Grüneisen ratio. Figure 5 reveals a practically temperature-independent ratio for the pressed-powder sample in the temperature range investigated. This is consistent with the notion that the low-energy excitation spectrum in the powder material is governed by a single energy scale, the pressure dependence of which is probed by Γ_p. We link this energy scale to the maximum in α and C_e at T_{max} around 1.4 K which reflects magnetic correlations in the strongly frustrated hyperkagome lattice. In contrast, for the single crystal, we find a distinctly different behavior. Whereas the ratio at higher temperatures lies close to the value for the powder material, it shows a distinctly different temperature dependence upon cooling. Of particular interest is the behavior at lowest temperatures where the influence of the phase transition anomalies in $\alpha_{[110]}$ and C_e around $T_{FE} \approx 1$ K is expected to be small, suggesting it is related to the magnetic sector. In fact, the data reveal a growing ratio $\alpha_{[110]}/C_e$ upon cooling for low temperatures. However, in light of the substantial error bars involved, the data do not allow to make a definite statement on the asymptotic behavior, especially whether or not this ratio diverges for $T \to 0$. In general,
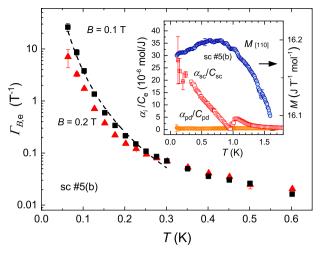
Fig. 5 Temperature dependence of the electronic magnetic Grüneisen parameter. Electronic magnetic Grüneisen parameter $\Gamma_{B,e}$ as a function of temperature for PbCuTe$_2$O$_6$ single crystal #5(b) in a semi-logarithmic representation. Raw data were taken by applying small field ramps of $\Delta B = \pm 0.03$ T on top of a dc field of $B = 0.1$ T (black squares) and 0.2 T (red triangles) applied along [110], see "Methods" and Supplementary Note 2 as well as ref. [42] for details on the technique applied. A minimum dc field of 0.1 T was used to avoid issues associated with remnant fields of the magnet. Broken line shows a fit T^m with $m = 3.9$ to the data for $T \leq 0.25$ K. Error bars result from averaging over field-up and field-down sweep. The inset (left ordinate) shows the ratio $a_{sc}/C_{sc} = a_{[110]}/C_{sc}$ for single crystal #5 (open red squares) and a_{pd}/C_{pd} for the pressed-powder sample pd #I (open orange spheres) both measured at $B = 0$. Errors are calculated from the errors of α and C. The inset also shows results for the magnetization $M(T)$ (right ordinate) per mole in a field of $B = 0.1$ T along the [110] direction of sc #5(b) obtained by ac-susceptibility measurements. Representative error bar, denoting standard deviation due to statistical treatment of raw data.

a diverging Grüneisen ratio $\Gamma_p = 1/T \cdot (\partial T/\partial p)_S$, measuring temperature contours at constant entropy S, is considered a clear signature of a nearby pressure (p)-sensitive quantum critical point[35]. This defining property results from the accumulation of entropy close to the quantum critical point.

As an alternative approach for probing potential quantum critical behavior associated with the system's magnetic degrees of freedom, we performed measurements of the magnetic Grüneisen parameter $\Gamma_B = 1/T \cdot (\partial T/\partial B)_S$[35] from which the electronic magnetic Grüneisen parameter $\Gamma_{B,e}$ has been extracted by taking into account the nuclear contributions, see "Methods" and Supplementary Note 2 as well as Supplementary Figs. 3 and 4. In fact, as shown in the main panel of Fig. 5, the data reveal a diverging $\Gamma_{B,e}$ on cooling over about one decade in temperature down to 0.06 K with an asymptotic behavior following a $\Gamma_{B,e} \propto T^{-m}$ dependence with $m \approx 3.9$ for $T \leq 0.25$ K. Note that an independent determination of $\Gamma_{B,e}$ is provided by using the identity $\Gamma_{B,e} = -(\mathrm{d}M/\mathrm{d}T)/C_e$[35]. In fact, the calculation of $\Gamma_{B,e}$ based on the $M(T)$ data (inset of Fig. 5) and $C_e(T)$ data (Fig. 1), yields an almost identical behavior for $\Gamma_{B,e}(T)$ within the experimental uncertainty, see Fig. 4 in the Supplementary, that is, a divergence for $T \to 0$. From these observations, we conclude that single crystalline PbCuTe$_2$O$_6$ for $T \to 0$ approaches a quantum critical point which is sensitive to magnetic fields. This is consistent with results taken on mildly increasing the magnetic field to $B = 0.2$ T (Fig. 5), and the variation of $\Gamma_{B,e}$ with field measured at a constant temperature of $T = 0.15$ K (see Supplementary Fig. 5), yielding a suppression of $\Gamma_{B,e}$ following a $\Gamma_{B,e} = -A/(B - B_c)$ dependence with $A = 0.058 \pm 0.005$ and $B_c \approx 0$. According to ref. [35] this behavior is expected for a quantum paramagnetic state, that is, a non-critical spin-correlated state. This raises the question about the origin of the quantum critical

behavior that gives rise to the divergence in $\Gamma_{B,e}(T)$ at small fields. In light of the strong response revealed for the uniaxial thermal Grüneisen parameter along the [110] direction, we associate the quantum critical behavior to an instability of the quantum spin liquid against uniaxial pressure $p_{[110]}$ and the associated lattice distortions. It remains to be shown by future experiments on mono-domain single crystals whether or not there are divergences in the uniaxial thermal Grüneisen parameters also along the orthogonal [1–10] and [001] directions. Remarkably, an anisotropic thermal expansion response with quantum critical behavior only along one direction was observed for the heavy fermion metal CeRhSn[36] featuring a frustrated 2D kagome lattice.

In conclusion, comprehensive investigations on PbCuTe$_2$O$_6$ including thermodynamic, magnetic and dielectric probes, reveal markedly different behavior for single crystalline material as compared to pressed-powder samples: whereas the low-temperature properties of the powder material are consistent with the recently proposed gapless quantum spin liquid state, an even more exotic behavior is observed for the single crystals. Here, we find a ferroelectric transition at $T_{FE} \approx 1$ K, accompanied by pronounced lattice distortions, and somewhat modified magnetic signatures—still consistent with a quantum spin liquid—but with clear indications for quantum critical behavior. These findings call for low-temperature structural investigations on single crystals as key input for determining their T-dependent exchange interactions. It would be interesting to extend these low-temperature structural investigations also to the pressed-powder samples, as the non-critical behavior observed there is assigned to the lack of those lattice distortions.

In the absence of such low-T structural information, we speculate that the lattice distortions in single crystalline material and the associated changes in the electronic structure are likely to alter the magnetic network in a way that drives the system close to a quantum critical point. Based on the trend revealed by comparing the maximum in the specific heat at T_{max} for various frustrated antiferromagnets[13], we are inclined to assign the reduction of T_{max} from 1.4 K for the powder to below 1 K for the single crystals to an increase in the degree of frustration, thereby driving the system quantum critical. It is interesting to note that quantum critical behavior, assigned to geometrical frustration, has been observed also in other materials where a 3D frustrated spin system interacts with charge degrees of freedom such as in the Kondo lattice Pr$_2$Ir$_2$O$_7$[37] or the valence fluctuator β-YbAlB$_4$[38].

In contrast to these systems, PbCuTe$_2$O$_6$ features a spin system which is devoid of effects related to strong spin-orbit interactions, crystalline electric fields or Kondo-type interaction with delocalized charges. Thus, single crystalline PbCuTe$_2$O$_6$ offers the possibility for exploring quantum criticality resulting from a strongly frustrated hyperkagome spin system interacting with ferroelectricity—a scenario holding promise for fascinating physics. Especially, through comparison with the non-critical behavior of the undistorted low-T state realized in the pressed-powder samples of PbCuTe$_2$O$_6$, one may expect to find interesting magneto-electric coupling effects mediated by the lattice deformations.

METHODS

Samples investigated
Single crystals of PbCuTe$_2$O$_6$ were grown by utilizing two different techniques: a traveling solvent floating zone (TSFZ) method for sc #1, sc #2, and sc #4, and a top-seeded solution growth (TSSG) technique for sc #5. Details of the growth conditions and the sample characterization, including polarized optical microscopy, X-ray Laue and X-ray powder diffraction, are given in ref. [23]. According to these studies, the room-temperature structure of the resulting single crystals can be best refined in a cubic structure with space group P4$_1$32 and a lattice parameter $a = 12.4967$ Å (TSSG) and 12.502 Å (TSFZ), in agreement with previous results[18]. Whereas the single crystals grown by the TSFZ technique may contain non-magnetic foreign phases with a volume fraction of 8% at maximum, no foreign phase could be detected in these measurements for the crystals

grown by using the TSSG method. The pressed-powder samples were obtained by using "polycrystalline ceramic powder" from the solid-state reaction of the precursor oxides, as described in Note 3 of the Supplementary of ref. [20]. The powder was pressed into a pellet of 1 cm diameter by applying hydrostatic force up to 12 tons (~1.5 GPa). The starting material of the pressed-powder samples studied here, i.e., the ceramic powder of $PbCuTe_2O_6$, is taken from the same batch as the "polycrystalline samples" characterized and investigated via neutron scattering and synchrotron diffraction in ref. [20]. According to these characterization measurements the powder is phase pure with a room-temperature structure of $P4_132$ space group and a lattice constant $a = 12.4968(4)$ Å, see Supplementary of ref. [20], consistent with the above results for the single crystals. In addition, the influence of the preparation conditions of polycrystalline materials on the thermal properties was studied in ref. [23], and no effects of off-stoichiometry on the cation sites or oxygen deficiency could be observed.

Thermal expansion

Thermal expansion experiments were performed by using a homemade capacitive dilatometer following the design discussed in ref. [39]. In this technique, relative length changes $\Delta L(T)/L$ are measured with $\Delta L(T) = L(T) - L(T_0)$ and T_0 the starting temperature of the experiment. Measurements were performed at temperatures $0.05\,K \leq T \leq 2\,K$, using a bottom-loading ^{3}He-^{4}He dilution refrigerator and for $1.5\,K \leq T \leq 200\,K$, using a ^{4}He-bath cryostat. In the dilatometer cell used, the spring leafs suspending the movable part exert a force **F** to the sample along the measuring direction with $F \approx 0.03\,N$–$3\,N$, the actual strength of which depends on the chosen starting capacitance. This results in uniaxial pressure along the measuring direction $p_{ua} = F/A$ with A the cross-sectional area of the sample, typically ranging from $p_{ua} \approx 0.01\,MPa$ to $5\,MPa$.

Specific heat

The specific heat measurements were carried out by employing both a homemade relaxation calorimeter as well as a homemade continuous-heating-type calorimeter both of which were attached to a bottom-loading ^{3}He-^{4}He dilution refrigerator. In the measurements of the specific heat at low temperatures $T < 1.6\,K$, basically two different contributions have to be considered. The electronic contribution of interest here, C_e, arises from the magnetic moments associated with the spins of the 3d electrons of the Cu^{2+} ions. The second one, C_n, is due to the magnetic moments of the ^{207}Pb, ^{125}Te, ^{63}Cu, and ^{65}Cu nuclei present in $PbCuTe_2O_6$. The phonon contribution C_{ph}, however, is negligibly small and does not exceed 1 % of C_e for $T < 1.6\,K$, see ref. [18]. Below $T \approx 0.1\,K$ the nuclear contribution dominates (see Note 2 and Fig. 2 of the Supplementary) and has to be determined quite accurately in order to extract C_e reliably from the measured total specific heat C. The contributions of the various nuclei, $C_{n,i}$, are Schottky anomalies resulting from the splitting of energy levels in a magnetic field. In the case of the ^{207}Pb and ^{125}Te nuclei, this field is identical to the external magnetic field, as there are no electronic magnetic moments in the immediate vicinity. Thus $C_{n,i}$ can be calculated easily by using the corresponding parameters from literature (refs. [40,41]), that is, the natural abundances of the various isotopes, their nuclear spins and associated nuclear magnetic moments (see also Supplementary Table 1). For the copper nuclei, however, the local field is strongly influenced by the magnetic field caused by the magnetic moment of the 3d electrons of the Cu^{2+} ion. Therefore, this local field has to be determined by a $1/T^2$ fit to the low-temperature specific heat data in $B = 0$, yielding a local electronic field of $B_e \approx 10.2\,T$, see also Supplementary Note 2 for details.

Magnetic Grüneisen parameter

The magnetic Grüneisen parameter, $\Gamma_B = T^{-1} \cdot (\partial T/\partial B)_S$, was measured by using a relaxation calorimeter attached to a bottom-loading ^{3}He-^{4}He dilution refrigerator. For details of the applied technique, in which Γ_B is approximated by $\Gamma_B \approx T_s^{-1} \cdot (\Delta T_s/\Delta B)_{S \approx const.}$, see ref. [42]. Here T_s is the sample temperature, and ΔT_s the temperature change induced in response to changes in the applied magnetic field ΔB.

The electronic magnetic Grüneisen parameter $\Gamma_{B,e}$ can be extracted from the measured magnetic Grüneisen parameter Γ_B of the total system by taking the specific heat contributions C_i and magnetic Grüneisen parameters $\Gamma_{B,i}$ of all relevant subsystems into account: $\Gamma_B = \frac{1}{C} \cdot \sum_i C_i \cdot \Gamma_{B,i}$, with $C = \sum_i C_i$ the total specific heat. In the case of

$PbCuTe_2O_6$, $\Gamma_{B,e}$ is then given by (see also Supplementary Note 2):

$$\Gamma_B = \frac{1}{C} \cdot (C_e \cdot \Gamma_{B,e} + C_{nPb} \cdot \Gamma_{B,nPb} + C_{nTe} \cdot \Gamma_{B,nTe} + C_{nCu} \cdot \Gamma_{B,nCu}). \quad (1)$$

The nuclear magnetic moments of Te and Pb behave as Langevin paramagnets (for which the entropy $S = S(T/B)$ with the local magnetic field being identical to the external magnetic field, so that $\Gamma_{B,nPb} = \Gamma_{B,nTe} = 1/B$. For $\Gamma_{B,nCu}$ the situation is more complex due to the strong influence of the magnetic field caused by the magnetic moment of the 3d electrons on the local magnetic field acting on the nuclei In the absence of magnetic ordering, and for not too large magnetic fields, the following expression can be derived for the determination of $\Gamma_{B,e}$ (see Supplementary Note 2 for details):

$$\Gamma_{B,e} = \frac{1}{C_e} \cdot \left[C \cdot \Gamma_B - (C_{nPb} + C_{nTe}) \cdot \frac{1}{B} - C_{nCu} \cdot \frac{B}{3B_e^2} \right]. \quad (2)$$

Dielectric measurements

For measurements of the dielectric constant, a plate capacitor arrangement was realized by attaching two electrodes (silver paste) to opposite parallel surfaces of the samples. The dielectric constant was derived from the capacitance, read out by using an LCR meter (Agilent E4980), and the geometrical dimensions of the plate capacitor. This procedure implies an uncertainty in the experimental data of about ±5%. Measurements were performed by using a top-loading ^{3}He-^{4}He dilution refrigerator.

Polarization

The polarization measurements were performed using the same capacitor-contact geometry as described for the dielectric measurements. To determine the ferroelectric polarization, standard pyrocurrent experiments were performed by prepoling the sample upon cooling down to 0.9 K with different applied electrical fields and subsequent monitoring of the pyrocurrent under heating beyond the transition temperature. The pyrocurrent was recorded using a Keysight B2987A electrometer and applying a heating rate of 60 mK/min. For examples of pyrocurrent measurements see Note 8 and Fig. 10 of the Supplementary. The polarization was deduced by integration of the pyrocurrent over time. To check for the switchability of the polarization, additional experiments were performed by (i) measuring the pyrocurrent upon cooling the sample with applied electrical field, (ii) subjecting the sample to a field of opposite direction for 1 min after reaching a base temperature of 0.9 K, and (iii) monitoring the pyrocurrent upon subsequent heating in zero field. Typical fields applied were of the order of several kV/cm.

Ac-susceptibility

For measurements of the ac-susceptibility, a homemade susceptometer adapted to a top-loading ^{3}He-^{4}He dilution refrigerator was employed. The ac-susceptometer was calibrated via magnetization measurements up to 5 T by comparing the results with data obtained by using a SQUID magnetometer (Quantum Design MPMS).

DATA AVAILABILITY

All the raw and derived data that support the findings of this study are available from the authors upon reasonable request.

REFERENCES

1. Balents, L. Spin liquids in frustrated magnets. *Nature* **464**, 199–208 (2010).
2. Lacroix, C., Mendels, P. & Mila, F. Introduction to Frustrated Magnetism. Springer Series in Solid-State Sciences Vol. **164** (Springer, New York, 2011).
3. Savary, L. & Balents, L. Quantum spin liquids: a review. *Rep. Prog. Phys.* **80**, 016502 (2017).
4. Zhou, Y., Kanoda, K. & Ng, T.-K. Quantum spin liquid states. *Rev. Mod. Phys.* **89**, 025003 (2017).
5. Broholm, C. et al. Quantum spin liquids. *Science* **367**, eaay0668 (2020).
6. Helton, J. S. et al. Spin dynamics of the spin-1/2 Kagome lattice antiferromagnet $ZnCu_3(OH)_6Cl_2$. *Phys. Rev. Lett.* **98**, 107204 (2007).

7. Han, T.-H. et al. Fractionalized excitations in the spin-liquid state of a kagome-lattice antiferromagnet. *Nature* **492**, 406–410 (2012).

8. Shimizu, Y. et al. Spin liquid state in an organic Mott insulator with a triangular lattice. *Phys. Rev. Lett.* **91**, 107001 (2003).

9. Itou, T. et al. Quantum spin liquid in the spin-1/2 triangular antiferromagnet EtMe$_3$Sb[Pd(dmit)$_2$]$_2$. *Phys. Rev. B* **77**, 104413 (2008).

10. Powell, B. J. & McKenzie, R. H. Quantum frustration in organic Mott insulators: from spin liquids to unconventional superconductors. *Rep. Prog. Phys.* **74**, 056501 (2011).

11. Gardner, J. S., Gingras, M. J. P. & Greedan, J. E. Magnetic pyrochlore oxides. *Rev. Mod. Phys.* **82**, 53 (2010).

12. Rau, J. G. & Gingras, M. J. P. Frustrated quantum rare-earth pyrochlores. *Annu. Rev. Condens. Matter Phys.* **10**, 357–386 (2019).

13. Okamoto, Y., Nohara, M., Aruga-Katori, H. & Takagi, H. Spin-liquid state in the $S = 1/2$ hyperkagome antiferromagnet Na$_4$Ir$_3$O$_8$. *Phys. Rev. Lett.* **99**, 137207 (2007).

14. Elhajal, M., Canals, B. & Lacroix, C. Symmetry breaking due to Dzyaloshinsky-Moriya interactions in the kagome lattice. *Phys. Rev. B* **66**, 014422 (2002).

15. Cépas, O., Fong, C. M., Leung, P. W. & Lhuillier, C. Quantum phase transition induced by Dzyaloshinskii-Moriya interactions in the kagome antiferromagnet. *Phys. Rev. B* **78**, 140405(R) (2008).

16. Chen, G. & Balents, L. Spin-orbit effects in Na$_4$Ir$_3$O$_8$: a hyper-kagome lattice antiferromagnet. *Phys. Rev. B* **78**, 094403 (2008).

17. Singh, Y., Tokiwa, Y., Dong, J. & Gegenwart, P. Spin liquid close to a quantum critical point in Na$_4$Ir$_3$O$_8$. *Phys. Rev. B* **88**, 220413(R) (2013).

18. Koteswararao, B. et al. Magnetic properties and heat capacity of the three-dimensional frustrated $S = 1/2$ antiferromagnet PbCuTe$_2$O$_6$. *Phys. Rev. B* **90**, 035141 (2014).

19. Khuntia, P. et al. Spin liquid state in the 3D frustrated antiferromagnet PbCuTe$_2$O$_6$: NMR and Muon spin relaxation studies. *Phys. Rev. Lett.* **116**, 107203 (2016).

20. Chillal, S. et al. Evidence for a three-dimensional quantum spin liquid in PbCuTe$_2$O$_6$. *Nat. Commun.* **11**, 2348 (2020).

21. Weil, M., Shirkhanlou, M. & Stürzer, T. Phase formation studies of lead(II) copper(II) oxotellurates: the crystal structures of dimorphic PbCuTeO$_5$, PbCuTe$_2$O$_6$, and [Pb$_2$Cu$_2$(Te$_4$O$_{11}$)](NO$_3$)$_2$. *Z. Anorg. Allg. Chem.* **645**, 347–353 (2019).

22. Koteswararao, B. et al. Observation of $S = \frac{1}{2}$ quasi-1D magnetic and magneto-dielectric behavior in a cubic SrCuTe$_2$O$_6$. *J. Phys.: Condens. Matter* **27**, 426001 (2015).

23. Hanna, A. R. N. et al. Crystal growth, characterization, and phase transition of PbCuTe$_2$O$_6$. *Phys. Rev. Mater.* **5**, 113401 (2021).

24. Köppen, M. et al. Solitary magnetic excitations in the low-carrier density, one-dimensional $S = 1/2$ antiferromagnet Yb$_4$As$_3$. *Phys. Rev. Lett.* **82**, 4548–4551 (1999).

25. Lines, M. E. & Glass, A. M. *Principles and Application of Ferroelectrics and Related Materials* (Clarendon Press, Oxford, 1977).

26. Lunkenheimer, P. et al. Multiferroicity in an organic charge-transfer salt that is suggestive of electric-dipole-driven magnetism. *Nat. Mater.* **11**, 755–758 (2012).

27. Lu, J. et al. On the room temperature multiferroic BiFeO$_3$: magnetic, dielectric and thermal properties. *Eur. Phys. J. B* **75**, 451–460 (2010).

28. Wieder, H. H. Electrical behavior of barium titanate single crystals at low temperatures. *Phys. Rev.* **99**, 1161–1165 (1955).

29. Tokura, Y., Seki, S. & Nagaosa, N. Multiferroics of spin origin. *Rep. Prog. Phys.* **77**, 076501 (2014).

30. Zhong, W. L. et al. Phase transition in PbTiO$_3$ ultrafine particles of different sizes. *J. Phys.: Condens. Matter* **5**, 2619–2624 (1993).

31. Chattopadhyay, S., Ayyub, P., Palkar, V. R. & Multani, M. Size-induced diffuse phase transition in the nanocrystalline ferroelectric PbTiO$_3$. *Phys. Rev. B* **52**, 13177–13183 (1995).

32. Zhao, Z. et al. Grain-size effects on the ferroelectric behavior of dense nano-crystalline BaTiO$_3$ ceramics. *Phys. Rev. B* **70**, 024107 (2004).

33. Nakatsuji, S. et al. Spin disorder on a triangular lattice. *Science* **309**, 1697–1700 (2005).

34. Cheng, J. G. et al. High-pressure sequence of Ba$_3$NiSb$_2$O$_9$ structural phases: new $S = 1$ quantum spin liquids based on Ni^{2+}. *Phys. Rev. Lett.* **107**, 197204 (2011).

35. Zhu, L., Garst, M., Rosch, A. & Si, Q. Universally diverging Grüneisen parameter and the magnetocaloric effect close to quantum critical points. *Phys. Rev. Lett.* **91**, 066404 (2003).

36. Tokiwa, Y. et al. Characteristic signatures of quantum criticality driven by geometrical frustration. *Sci. Adv.* e1500001 (2015).

37. Tokiwa, Y., Ishikawa, J. J., Nakatsuji, S. & Gegenwart, P. Quantum criticality in a metallic spin liquid. *Nat. Mater.* **13**, 356–359 (2014).

38. Matsumoto, Y. et al. Quantum criticality without tuning in the mixed valence compound β-YbAlB$_4$. *Science* **331**, 316–319 (2011).

39. Pott, R. & Schefzyk, R. Apparatus for measuring the thermal expansion of solids between 1.5 and 380 K. *J. Phys. E* **16**, 444–449 (1983).

40. Fuller, G. H. Nuclear spins and moments. *J. Phys. Chem. Ref. Data* **5**, 835–1092 (1976).

41. De Bièvre, P. & Taylor, P. D. P. Table of the isotopic compositions of the elements. *Int. J. Mass Spectrom. Ion-. Process.* **123**, 149–166 (1993).

42. Wolf, B. et al. Magnetocaloric effect and magnetic cooling near a field-induced quantum-critical point. *Proc. Natl Acad. Sci. USA* **108**, 6862–6866 (2011).

43. Kittel, Ch. *Introduction to Solid State Physics* (7th ed.) (John Wiley & Sons, Inc, New York, 1996).

44. Gati, E. et al. Evidence for electronically driven ferroelectricity in a strongly correlated dimerized BEDT-TTF molecular conductor. *Phys. Rev. Lett.* **120**, 247601 (2018).

ACKNOWLEDGEMENTS

AUTHOR CONTRIBUTIONS

B.L., S.C., B.W., and M.L. planned the project. Measurements and analysis of specific heat and magnetic Grüneisen parameter were performed by P.E. and U.T. Measurements and analysis of thermal expansion were performed by C.T., Y.S., S. H., B.W., and M.L. Measurements and analysis of the magnetic susceptibility were performed by B.W. and P.E. Measurements and analysis of the dielectric constant were performed by A.A. and U.T. Measurements and analysis of ultrasonic experiments were performed by J.Z. and B.W. Measurements of electric polarization were performed by M.W., B.W., and A.A. The data were discussed and analyzed by M.W., P.L., and I.K. The samples were synthesized and characterized by A.R.N.H., S.C., A.T.M.N.I., and B.L. B.W. and M.L. discussed the results and prepared the manuscript.

FUNDING

COMPETING INTERESTS

The authors declare no competing interests.

ADDITIONAL INFORMATION

Supplementary information The online version contains supplementary material available at https://doi.org/10.1038/s41535-021-00395-6.

Correspondence and requests for materials should be addressed to Christian Thurn.

Reprints and permission information is available at http://www.nature.com/reprints

Publisher's note Springer Nature remains neutral with regard to jurisdictional claims in published maps and institutional affiliations.